JOURNAL OF APPLIED ELECTROCHEMISTRY 22 (1992) 596–605

Effect of gas sparging on mass transfer in zinc electrolytes

A. Y. HOSNY, T. J. O'KEEFE, J. W. JOHNSON, W. J. JAMES

Departments of Chemical Engineering, Metallurgical Engineering, and Chemistry and Graduate Center for Materials Research, University of Missouri-Rolla, Rolla, Missouri, 65401, USA

Received 10 July 1990; revised 9 July 1991

The effect of sparging on mass transfer is reported for zinc electrolytes containing antimony and antimony-free electrolytes. Comparative results with non-sparged electrolytes show an enhancement in mass transfer. In the sparged electrolyte, the mass transfer coefficients, K_{Zn}, increase with increasing current density, antimony additions, and sulphuric acid concentration. The deposition morphology is consistent with the mass transfer results. A relationship between the mass transfer coefficients for sparged and non-sparged systems is obtained. The relationship correlates satisfactorily with the data and provides a quantitative method for determining the degree of enhancement in mass transfer coefficients due to sparging. The correlation which best represents the mass transfer data for sparged zinc electrolytes is

$$Sh = 105(ReSc)^{0.23}$$

where *Sh*, *Re*, and *Sc* are the Sherwood, Reynolds, and Schmidt numbers, respectively. The correlation represents the case where sparging is applied to a gas evolving electrode, hydrogen in this case.

1. Introduction

In electrochemical industries, such as zinc electrowinning, it is preferable to have a high production rate per unit volume of reactor. Irregular growth of deposits can occur, however, when the plating current density exceeds a certain fraction of the limiting current [1]. Therefore, an increase in the limiting current density is desirable for industrial applications in order to obtain a smooth deposit at a relatively higher deposition rate. In electrolytic cells, stirring by means of gas bubbles is an efficient method whereby enhanced mass transfer can result without sacrificing deposit morphology [2, 3].

Mass transfer studies using gas stirring have recently received considerable attention as a means of enhancing mass transfer rates [4–11]. Literature studies indicate that there are several types of gas-stirring processes which may be classified as follows:

(i) stirring by gas-evolving electrodes where gas evolves at the working electrode simultaneously with the main reaction [2, 5];

(ii) gas-sparged electrodes where the electrolyte is stirred by gas introduced from the outside into the cell through a distributor [2, 3, 6, 7]; and

(iii) electrodes stirred by gases which evolve at the counter electrode [8–11].

There is extensive literature regarding gas-evolving electrodes. However, relatively few comprehensive studies of gas-sparged electrodes are available. A sparging gas increases the mass transport and provides a uniform mass transfer coefficient over the entire electrode height [6]. It is important to note that most gas-sparged electrode studies reported in the literature are for electrodes where gas does not evolve at their surfaces. Furthermore, sparging gases are usually inert, e.g. nitrogen, and are introduced either at larger flow rates or at smaller volumes relative to the volumes of gases evolving at the electrodes.

Superposition of electrolyte flow on gas-sparged electrodes has been discussed recently [2, 3]. The mass transfer coefficients are enhanced when increasing electrolyte flow is imposed on the working electrode [2]. In the present research an outside gas flow of nitrogen, instead of the electrolyte flow, was superimposed on a gas-evolving electrode (hydrogen gas evolved at the working electrode simultaneously with zinc deposition).

Direct determination of the zinc limiting current density is difficult to achieve due to hydrogen evolution and surface roughness. Ettel [6] developed a useful technique for determining mass transfer coefficients (K) in electrowinning cells by measuring the mass transfer coefficients of a tracer. The technique was applied more recently [2, 12]. The tracer must be more noble than the bulk electrolyte cation and must be deposited at its limiting current density during the deposition process time of the cation species. The mass transfer coefficients of the main species were calculated for a forced flow from the following equation:

$$K_{\text{main ion}} = K_{\text{tracer}}(D_{\text{main ion}}/D_{\text{tracer}})^{0.66} \quad (1)$$

where D is the diffusion coefficient. In the present research, Cd was used as a tracer ion since it is more

0021-891X/92

noble than the zinc ion. Chemical analyses were carried out to obtain the Cd limiting current density and subsequently the mass transfer. Accordingly, the zinc mass transfer coefficients were determined. In this study, we report the effect of the sparging gas on the mass transfer coefficients and the deposition morphologies. The research was conducted for antimony-free and antimony-containing electrolytes in order to investigate the effect of sparging on antimony behaviour in the electrolyte.

Very few models or empirical correlations are available for sparged systems. The hydrodynamic model described by Janssen and Hoogland [13] is based on the mass transfer for natural turbulent convection. For a constant drag coefficient, the final presentation of the model [5] is given by

$$Sh = \text{constant } (ReSc)^{0.33} \quad (2)$$

where Sh is the Sherwood number (KL/D), Re the Reynolds number (Lv/ν), Sc the Schmidt number (ν/D), K the mean mass transfer coefficient (cm s^{-1}), L the characteristic length of the electrode (cm), D the diffusion coefficient (cm^2 s^{-1}), v the discharge velocity (cm s^{-1}), and ν the solution viscosity (cm^2 s^{-1}). The model takes into account the flow effects induced by bubbles rising near the electrode. However, the model does not distinguish between gas-evolving and gas-sparged electrodes [5].

A model proposed by Sigrist *et al.* [3] is based upon turbulent convection, and requires a previous measurement of the gas void fraction, ε. The electrolytic gas evolution is simulated by a vertical porous plate through which gas enters the cell. The model is given by

$$Sh = 0.19\ (ScAr)^{0.33} \quad (3)$$

where Ar is the modified Archimedes number specified by $(Lg/\nu^2)(\varepsilon/1 - \varepsilon)$. The term ε refers to the gas voidage fraction, and g the acceleration due to gravity (cm s^{-2}).

A more recent model described in the literature [4] is based upon a theoretical approach which assumes that eddies are primarily responsible for the enhancement of mass transfer. The model is given by

$$StSc^{0.5} = 0.035\ (FrRe)^{-0.25} \quad (4)$$

where St is the Stanton number (K/vL) and Fr the Froude number (v^2/Lg).

The objectives of the present study were to determine the degree of enhancement in mass transfer due to sparging as an alternative method for stirring the electrolyte, to obtain an overall correlation in dimensionless form suitable for practical applications, to evaluate the deposition morphology, particularly in the presence of antimony, and to present a relationship between the mass transfer coefficients for systems involving gas evolution and with systems involving additional superposition of a gas flow.

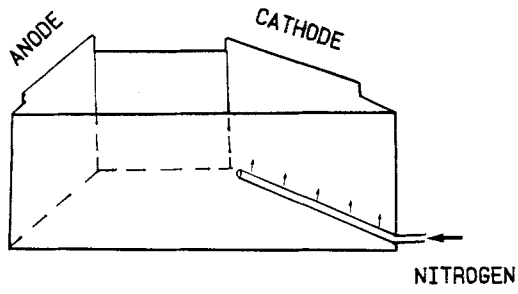

Fig. 1. Sparger position in the Hull cell.

2. Experimental details

A Hull cell (267 ml volume) with a sparger was used to carry out the experiments. The sparger was made of a perforated Teflon tube (10 holes, each with an area of 1.266×10^{-4} cm^2) placed at the bottom of the cathode as shown in Fig. 1. The sparger was attached to a flow meter and a nitrogen gas tank. The gas flow rate was kept constant at 2.25 dm^3 min^{-1}. The aluminum cathodes were prepared by a method described in [14] and connected to a power supply and a lead anode. The total current applied from the power supply was 2 A, providing current densities of 2 to 80 mA cm^{-2} at the cathode surface due to the special trapezoidal dimensions of the cell. The electrode working area was separated into several domains by electroplaters' tape, with each domain representing a range of current density. For practical reasons, the current densities at the end of a domain refer to the current density range, e.g. a section between 8 and 12 mA cm^{-2} is considered to have a value of 12 mA cm^{-2}. A commercial saturated Hg/Hg_2SO_4 reference electrode (0.65 V/SHE) was used. The duration of each experiment was 20 min at ambient temperature of about 25° C.

The mass transfer measurements were obtained by a tracer technique [2, 6] using 50 mg dm^{-3} Cd^{2+}. The deposits were analysed chemically, $^*K_{Cd}$ was measured and subsequently the ionic mass transfer of zinc, $^*K_{Zn}$, was calculated.

French process zinc oxide powder was used for the preparation of the zinc electrolyte by dissolving it in reagent grade sulphuric acid and deionized water. Antimony-potassium tartarate and cadmium sulphate were dissolved in deionized water to prepare stock solutions of Sb^{3+} and Cd^{2+}. Test solutions were prepared in a 1 dm^3 volumetric flask by mixing the proper amounts of neutral zinc sulphate solution, reagent grade sulphuric acid, Sb^{3+}, Cd^{2+}, and deionized water. The kinematic viscosities of the electrolytes were measured with a size 50 Cannon-Fenske viscometer.

The deposits considered for chemical analysis were obtained at current densities of 12, 30, 40, 50, and 60 mA cm^{-2}. The deposition areas were measured precisely for calculation of the current efficiencies. The volume flux of hydrogen was calculated from current efficiency data and Faraday's law. The calculation

* Throughout this manuscript, K_{Cd}, K_{Zn}, δ_{Zn}, etc., the subscript refers to the metal ion, Cd^{2+}, Zn^{2+}.

procedure is the same as for non-sparged systems [14]. Results obtained from non-sparged systems are presented in this study for comparison with the sparged results. SEM micrographs were taken for deposits at current density values of 20 and 80 mA cm^{-2}. They are compared with some SEM micrographs of non-sparged systems.

3. Results and discussion

3.1. *An antimony addition study*

Figure 2 shows the effect of antimony additions on the zinc diffusion layer thickness, δ_{Zn}, at different current densities (12 to 60 mA cm^{-2}) for an electrolyte containing 50 g dm^{-3} Zn, 150 g dm^{-3} H_2SO_4. In this current density range, δ_{Zn} decreases with increasing antimony concentration in the electrolyte. For example, at a current density of 50 mA cm^{-2}, the δ_{Zn} values are 3.27 × 10^{-3}, 3.08 × 10^{-3}, and 2.67 × 10^{-3} cm for 0.0, 0.04, and 0.08 mg dm^{-3} antimony concentrations, respectively. At a constant sparging rate, the decrease in δ_{Zn} is due to the increase in hydrogen evolution at the cathode surface since the increase in the antimony concentration enhances hydrogen evolution which occurs simultaneously with zinc deposition. For example, the volume flux values at 50 mA cm^{-2} given in Tables 1, 2, and 3 are 8.13 × 10^{-2}, 10.03 × 10^{-2}, and 12.49 × 10^{-2} cm^{3}cm^{-2}min^{-1} for 0.0, 0.04, and 0.08 mg dm^{-3} Sb^{3+}, respectively. At a constant sparging rate, the results in Fig. 2 and Table 1 indicate that δ_{Zn} decreases with increasing current density. For example, δ_{Zn} decreases by 25% as the current density increases from 12 to 60 mA cm^{-2}. The decrease in δ_{Zn} is accompanied by an increase in the hydrogen volume flux, where the value at 60 mA cm^{-2} is 2.62 times that at 12 mA cm^{-2}. The decrease in δ_{Zn} due to the change in antimony concentration from 0.0 to 0.08 mg dm^{-3} is 22% where the hydrogen volume flux at 0.08 mg dm^{-3} Sb^{3+} is 1.53 times the value at 0.0 mg dm^{-3} Sb^{3+}. The results suggest that the hydrogen evolved at the electrode surface for a sparged system also contributes to the enhancement of mass transfer, although there is a large difference in the volumes of the hydrogen gas and the sparged gas. This is due to the fact that the hydrogen gas bubbles evolve inside the diffusion layer.

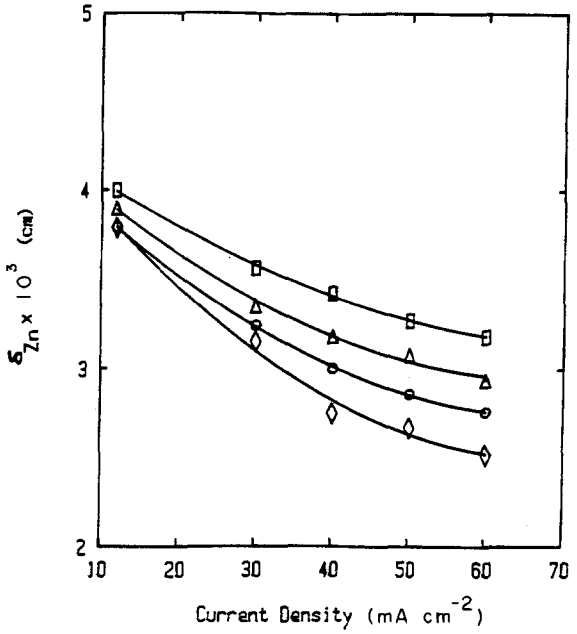

Fig. 2. Diffusion layer thickness of Zn obtained at different current densities for sparged electrolytes containing 50 g dm^{-3} Zn, 150 g dm^{-3} H_2SO_4, and various Sb^{3+} concentrations. [Sb^{3+}]: (□) 0.0, (△) 0.04, (○) 0.06 and (◇) 0.08 mg dm^{-3}.

Comparative results between sparged and non-sparged zinc electrolytes are shown in Figs 3 and 4, for the same electrolyte composition and electrolysis conditions. Figure 3 shows the effect of sparging on the zinc ionic mass transfer coefficients, K_{Zn}, at different antimony concentrations varying from 0.0 to 0.08 mg dm^{-3}, in an electrolyte of 50 g dm^{-3} Zn, 150 g dm^{-3} H_2SO_4 for current densities of 12, 30, and 60 mA cm^{-2}. It is found that there are significant increases in the K_{Zn} values when the system is sparged by nitrogen gas. For example, at 30 mA cm^{-2}, the K_{Zn} values are 11.49 × 10^{-4} and 5.63 × 10^{-4} cm s^{-1} for sparged and non-sparged systems, respectively, containing 0.04 mg dm^{-3} Sb^{3+}. The increase in the K_{Zn} values due to sparging is also observed at all antimony concentrations and in a 50 g dm^{-3} zinc electrolyte containing 200 g dm^{-3} H_2SO_4 as evidenced in Tables 4 and 5. Therefore, sparging with nitrogen is considered an effective method for enhancing the mass transport.

The effect of current density on the K_{Zn} values is shown in Fig. 4 for a 50 g dm^{-3} Zn electrolyte con-

Table 1. Calculation of Sc, Sh, and ScRe numbers for different plating current densities (c.d.) for a sparged electrolyte containing 50 g dm^{-3} Zn and 150 g dm^{-3} H_2SO_4

c.d. (mA cm^{-2})	*60*	*50*	*40*	*30*	*12*
$K_{Zn} \times 10^4$ (cm s^{-1})	11.9	11.6	11.1	10.6	9.5
$I_{l,Zn}$ (mA cm^{-2})	183.5	178.8	170.9	163.1	146.1
ρ (g cm^{-3})	1.142	1.147	1.153	1.158	1.169
$\nu \times 10^2$ (cm^{2}s^{-1})	1.460	1.491	1.521	1.552	1.610
$V_{H_2} \times 10^2$ (cm^{3}cm^{-2}min^{-1})	9.76	8.13	6.51	4.88	3.63
Sc	3839	3916	3992	4075	4247
Sh	470	458	438	418	374
$\delta_{Zn} \times 10^3$ (cm)	3.18	3.27	3.24	3.58	4.00
ScRe	642	535	428	321	239
ScGr × 10^{-9}	3.651	3.563	3.480	3.392	3.223

Table 2. Calculation of Sc, Sh, and ScRe numbers for different plating current densities (c.d.) for a sparged electrolyte containing 50 g dm^{-3} Zn, 150 g dm^{-3} H_2SO_4, and .04 mg dm^{-3} Sb^{3+}

c.d. (mA cm^{-2})	*60*	*50*	*40*	*30*	*12*
$K_{Zn} \times 10^4$ (cm s^{-1})	12.9	12.3	11.9	11.5	9.6
$I_{l,Zn}$ (mA cm^{-2})	198.7	189.6	183.7	176.8	148.5
ρ (g cm^{-3})	1.145	1.149	1.154	1.160	1.170
$v \times 10^2$ (cm^2 s^{-1})	1.470	1.501	1.530	1.560	1.610
$V_{H_2} \times 10^2$ (cm^3 cm^{-2} min^{-1})	12.03	10.03	8.02	6.02	4.54
Sc	3880	3943	4109	4099	4249
Sh	509	486	471	453	381
$\delta_{Zn} \times 10^3$ (cm)	2.94	3.08	3.18	3.13	3.94
ScRe	792	659	527	395	298
ScGr $\times 10^{-9}$	3.604	3.533	3.451	3.346	3.221

taining 150 g dm^{-3} H_2SO_4 and either none or 0.06 mg dm^{-3} antimony. The results show that the K_{Zn} values increase with increasing current density for the sparged system as well as for the non-sparged system. Two different stirring mechanisms are involved for enhancement of K_{Zn}, e.g. the first is an enhancement due to turbulent conditions resulting from sparging, the second is forced convection, existing in either sparged or non-sparged systems. The forced convection is due to the rising of the hydrogen bubbles which evolve simultaneously with Zn deposition at the electrode surface. Generally, the enhancement in the hydrogen rate is related to the increase in antimony concentration as the above results in Fig. 3 indicate, and also to the current density increase as shown in Fig. 4. For example, the K_{Zn} values for a sparged system change from 9.40 $\times$ 10^{-4} to 11.1 $\times$ 10^{-4} cm s^{-1} as the current density changes from 12 to 60 mA cm^{-2} for an antimony-free electrolyte containing 50 g dm^{-3} Zn and 150 g dm^{-3} H_2SO_4.

At 50 mA cm^{-2}, a striking increase in the K_{Zn} values is noticed due to sparging, for example K_{Zn} is increased by a factor of 2.25 when gas is sparged into an antimony-free electrolyte containing 50 g dm^{-3} Zn, 150 g dm^{-3} H_2SO_4. The corresponding K_{Zn} values are 4.7 $\times$ 10^{-4} and 10.6 $\times$ 10^{-4} cm s^{-1} for non-sparged and sparged electrolytes, respectively. Additionally, an increase in current density and/or antimony concentration increases K_{Zn}, for example K_{Zn} at 60 mA cm^{-2} is 1.2 times that of K_{Zn} at 12 mA cm^{-2} for an antimony-free electrolyte containing 50 g dm^{-3} Zn, 150 g dm^{-3} H_2SO_4. Furthermore, at a fixed current density of 50 mA cm^{-2}, K_{Zn} at 0.06 mg dm^{-3} Sb^{3+} is 1.17 times that of K_{Zn} at zero antimony for the same electrolyte.

Generally, for non-sparged systems, the growth of bubbles at the electrode surface stirs the electrolyte in a centrifugal fashion and microconvection flow develops in the vicinity of the bubbles [5]. On the other hand, for a sparged system, the gas velocity causes the flow to move parallel to the electrode surface and the well known phenomenon of macroconvection mass transfer develops. Both effects usually superimpose and enhance the mass transfer coefficients [15]. The effect of each case depends, among other factors, upon the amount of gas generated at the electrode surface and the gas sparging velocity. Therefore, it is not necessary for a volume of gas sparged into the system to have the same effect on mass transfer as an equal volume of gas evolved at the electrode surface due to the different mechanistic behaviour. Subsequently, the approach of the equal volume method used to study the effect of sparging needs to be carefully investigated for gas-evolving electrode systems. The present research represents an alternative method for future studies concerning mass transfer by sparging for such systems.

3.2. *Morphological studies*

For a sparged system, the effect of current density on deposition morphology for an electrolyte containing 50 g dm^{-3} Zn, 150 g dm^{-3} H_2SO_4 with an antimony

Table 3. Calculation of Sc, Sh, and ScRe numbers for different plating current densities (c.d.) for a sparged electrolyte containing 50 g dm^{-3} Zn, 150 g dm^{-3} H_2SO_4, and 0.08 mg dm^{-3} Sb^{3+}

c.d. (mA cm^{-2})	*60*	*50*	*40*	*30*	*12*
$K_{Zn} \times 10^4$ (cm s^{-1})	15.07	14.21	13.50	11.89	9.89
$I_{l,Zn}$ (mA cm^{-2})	231.9	218.5	209.4	182.9	152.2
ρ (g cm^{-3})	1.150	1.153	1.158	1.160	1.170
$v \times 10^2$ (cm^2 s^{-1})	1.501	1.520	1.550	1.561	1.620
$V_{H_2} \times 10^2$ (cm^3 cm^{-2} min^{-1})	14.99	12.49	10.10	7.49	5.11
Sc	3951	4000	4069	4109	4253
Sh	594	560	547	469	390
$\delta_{Zn} \times 10^3$ (cm)	2.52	2.67	2.73	3.19	3.84
ScRe	986	821	657	493	339
ScGr $\times 10^{-9}$	3.524	3.471	3.398	3.358	3.218

Table 4. Calculation of Sc, Sh, and ScRe numbers for different plating current densities (c.d.) for a sparged electrolyte containing 50 g dm^{-3} Zn, 100 g dm^{-3} H_2SO_4, and 0.02 mg dm^{-3} Sb^{3+}

c.d. (mA cm^{-2})	*60*	*50*	*40*	*30*	*12*
$K_{Zn} \times 10^4$ (cm s^{-1})	11.9	11.4	10.6	9.9	9.5
$I_{l,Zn}$ (mA cm^{-2})	187.6	178.5	166.7	155.8	149.3
ρ (g cm^{-3})	1.127	1.132	1.136	1.142	1.154
$v \times 10^2$ (cm^2 s^{-1})	1.410	1.430	1.450	1.470	1.522
$V_{H_2} \times 10^2$ (cm^3 cm^{-2} min^{-1})	9.99	8.32	6.66	4.99	3.74
Sc	3723	3765	3810	3866	4009
Sh	471	448	418	391	375
$\delta_{Zn} \times 10^3$ (cm)	3.18	3.34	3.58	3.83	3.99
ScRe	657	547	438	328	246
ScGr $\times 10^{-9}$	2.450	2.413	2.375	2.330	2.223

concentration of 0.06 mg dm^{-3} is shown in Figs 5a and b for current densities of 80 and 20 mA cm^{-2}, respectively. The surface deposition at 20 mA cm^{-2} shows a layered structure. This may be due to the presence of antimony and to hydrogen evolution. At a high deposition rate, 80 mA cm^{-2}, the surface exhibits a compact structure.

The effect of sparging on deposits obtained at a lower current density such as 20 mA cm^{-2} for a 50 g dm^{-3} Zn electrolyte containing 150 g dm^{-3} H_2SO_4 and 0.02 mg dm^{-3} Sb^{3+} is shown in Figs 6a and b for sparged and non-sparged systems, respectively. The sparged deposit is characterized by rounded edges and a relatively compact structure while in the non-sparged deposit, the edges are sharper. Therefore, the sparging may round the edges and compact the structure due to an enhancement in mass transport or to greater Zn dissolution. Figures 5a and 6a show the effect of an increase in antimony concentration on the morphology for sparged electrolytes. The increase in the Sb^{3+} concentration from 0.02 to 0.06 mg dm^{-3} increases the surface attack and causes zinc dissolution as shown in Fig. 6b for a non-sparged electrolyte containing 50 g dm^{-3} Zn, 150 g dm^{-3} acid at 20 mA cm^{-2}.

The SEM pictures for a 50 g dm^{-3} Zn electrolyte containing a higher acid concentration of 200 g dm^{-3} H_2SO_4 and a higher antimony concentration of 0.08 mg dm^{-3} at a current density of 20 mA cm^{-2} are shown in Fig. 7a and b for sparged and non-sparged systems, respectively. Both surfaces have deteriorated, however, the deposit obtained for the sparged system looks to be less attacked than that for the non-sparged deposit. The surface obtained in the non-sparged system is dissolving and some parts of the aluminium substrate, dark spots in the picture, can be seen. The grain boundaries are separated and holes can be observed. On the other hand, the surface obtained from the sparged system is relatively compact, less attacked, forms a layer structure and the edges are rounded. Since sparging enhances mass transport, it was expected that the deleterious effects of antimony on zinc deposition would be increased greatly for the sparged systems at the higher levels of antimony and acid concentration. However, the results are opposite to what was expected. Therefore, additional experiments were carried out separately in a regular electrolysis cell at a current density of 20 mA cm^{-2} under similar conditions, and the results indicate a similar trend and sustain our findings. At a low current density such as 20 mA cm^{-2} the surface morphology is affected by the rate of zinc deposition and the rate of zinc dissolution due to the presence of antimony. Sparging enhances both rates and subsequently, the order of magnitude is changed. Therefore, the Zn deposition rate may be more effective than the Zn dissolution rate at such higher acid and antimony concentrations.

SEM pictures obtained at a higher current density, 80 mA cm^{-2}, for the same conditions discussed above, 200 g dm^{-3} H_2SO_4 and 0.08 mg dm^{-3} Sb^{3+}, are shown in Fig. 8a and b for sparged and non-sparged systems,

Table 5. Calculation of Sc, Sh, and ScRe numbers for different plating current densities (c.d.) for a sparged electrolyte containing 50 g dm^{-3} Zn, 100 g dm^{-3} H_2SO_4, and 0.08 mg dm^{-3} Sb^{3+}

c.d. (mA cm^{-2})	*60*	*50*	*40*	*30*	*12*
$K_{Zn} \times 10^4$ (cm s^{-1})	14.0	13.2	12.4	11.5	9.9
$I_{l,Zn}$ (mA cm^{-2})	219.9	207.7	194.8	181.3	155.1
ρ (g cm^{-3})	1.133	1.136	1.140	1.145	1.154
$v \times 10^2$ (cm^2 s^{-1})	1.430	1.450	1.462	1.482	1.531
$V_{H_2} \times 10^2$ (cm^3 cm^{-2} min^{-1})	13.62	11.36	9.08	6.81	5.68
Sc	3773	3809	3851	3899	4013
Sh	552	521	489	455	389
$\delta_{Zn} \times 10^3$ (cm)	2.71	2.87	3.06	3.29	3.85
ScRe	896	747	597	448	373
ScGr $\times 10^{-9}$	2.406	2.376	2.342	2.304	2.220

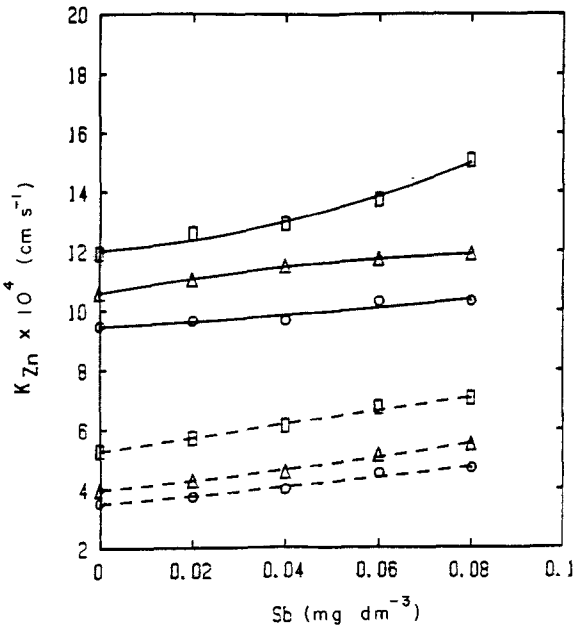

Fig. 3. The effect of the antimony concentration and the current density on the K_{Zn} for a sparged (——) and a non-sparged (– – –) electrolyte containing 50 g dm^{-3} Zn and 150 g dm^{-3} H_2SO_4. C.d.: (□) 60, (△) 30 and (○) 12 mA cm^{-2}.

respectively. Both deposits show a compact surface with no sign of dissolution. However, the grain boundaries in the case of sparging are more rounded than those in the non-sparged deposit. The results agree with mass transfer studies where the increase in current density enhances the K_{Zn} values. At the same current density of 80 mA cm^{-2}, the micrographs of deposits obtained from an antimony-free electrolyte containing 50 g dm^{-3} Zn and 200 g dm^{-3} H_2SO_4 are shown in Fig. 9a and b for sparged and non-sparged systems, respectively. The zinc facets are sharper

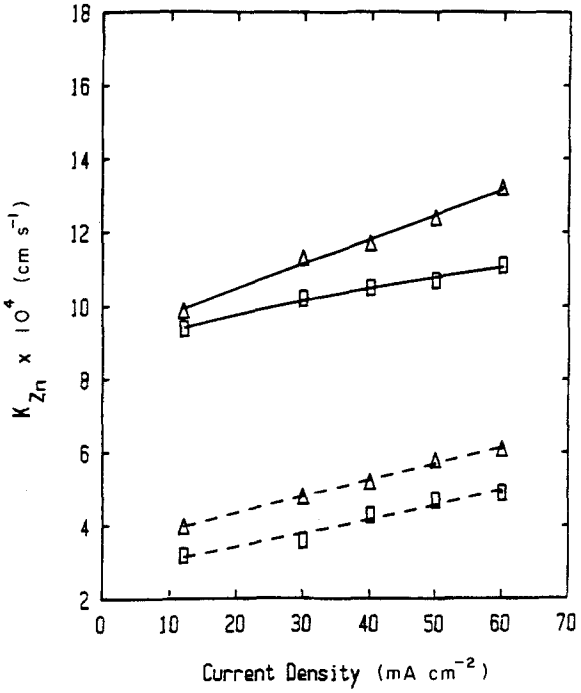

Fig. 4. Plot of the K_{Zn} against current density for a sparged (——) and a non-sparged (– – –) electrolyte containing 50 g dm^{-3} Zn and 100 g dm^{-3} H_2SO_4 with 0.0 (□) and 0.06 (△) mg dm^{-3} antimony.

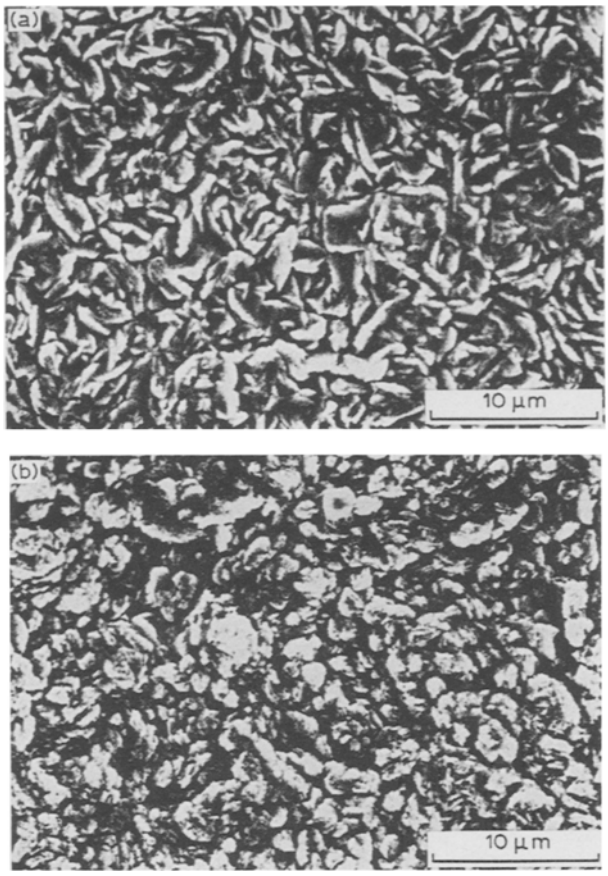

Fig. 5. Zinc deposits obtained for a sparged electrolyte containing 50 g dm^{-3} Zn, 150 g dm^{-3} H_2SO_4, and 0.06 mg dm^{-3} Sb^{3+}. (a) 20 and (b) 80 mA cm^{-2}.

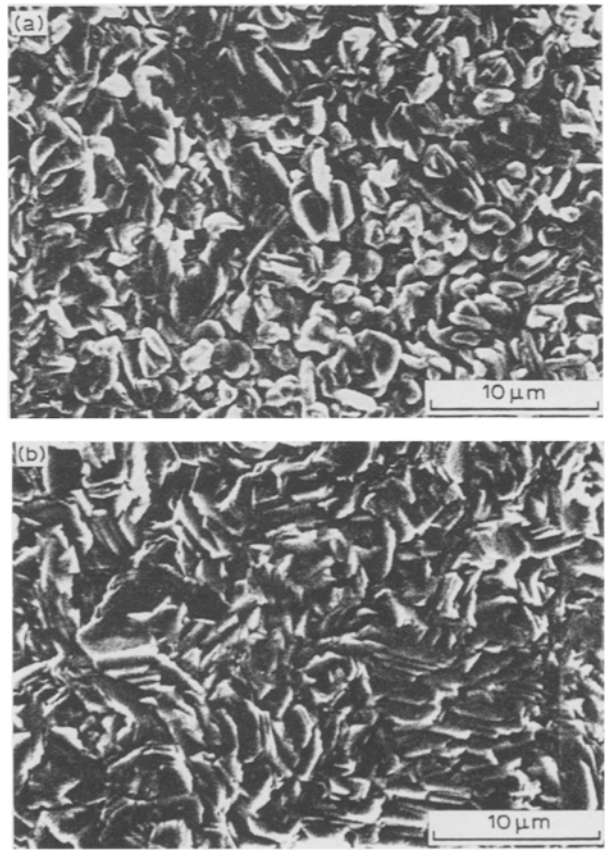

Fig. 6. Zinc deposits obtained at 20 mA cm^{-2} for an electrolyte containing 50 g dm^{-3} Zn, 150 g dm^{-3} H_2SO_4, and 0.02 mg dm^{-3} Sb^{3+}. (a) Sparged and (b) not sparged.

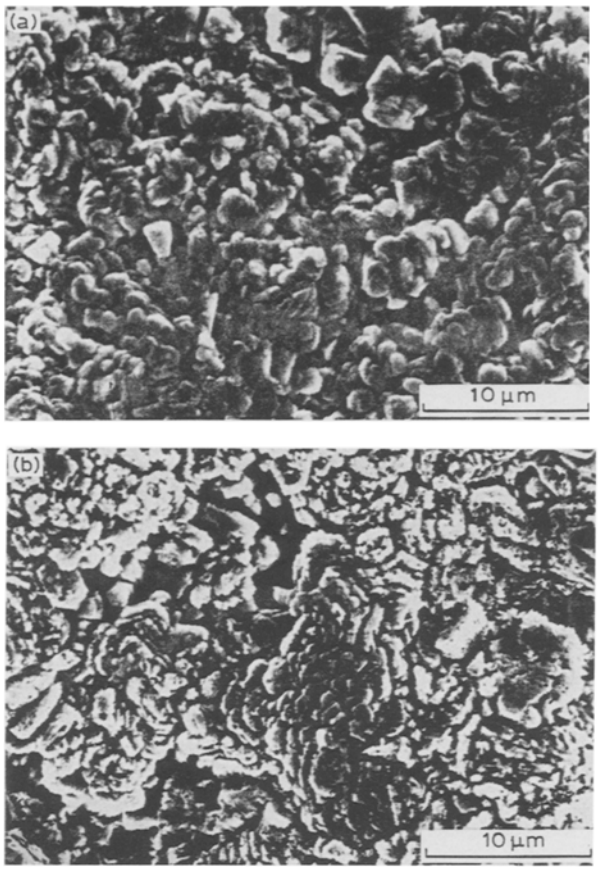

Fig. 7. Zinc deposits obtained at 20 mA cm^{-2} for an electrolyte containing 50 g dm^{-3} Zn, 200 g dm^{-3} H_2SO_4, and 0.08 mg dm^{-3} Sb^{3+}. (a) Sparged and (b) not sparged.

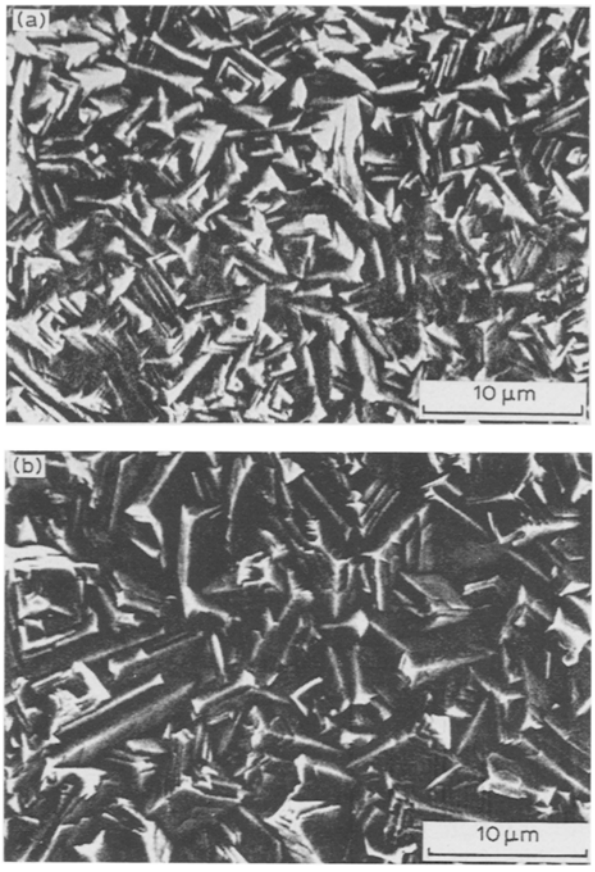

Fig. 9. Zinc deposits obtained at 80 mA cm^{-2} for an antimony-free electrolyte containing 50 g dm^{-3} Zn and 200 g dm^{-3} H_2SO_4. (a) Sparged and (b) not sparged.

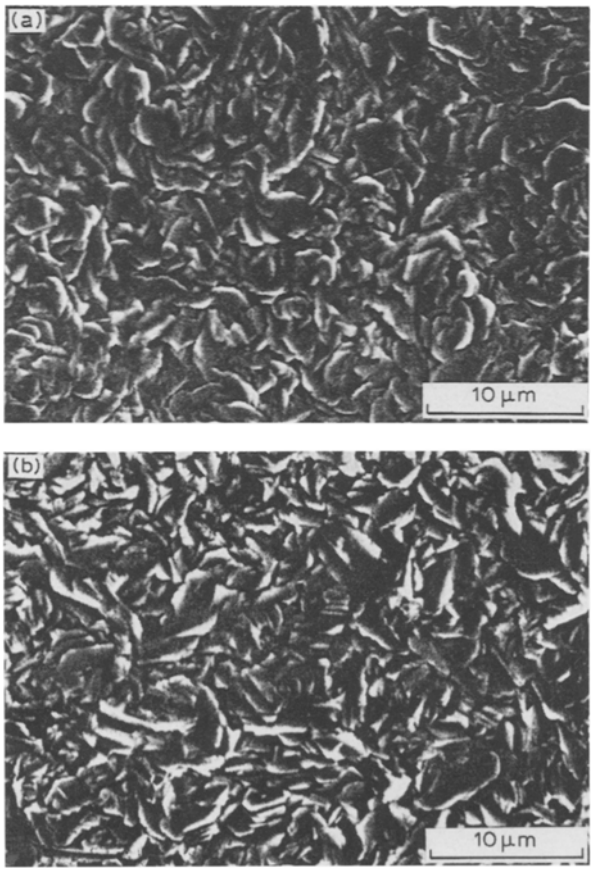

Fig. 8. Zinc deposits obtained at 80 mA cm^{-2} for an electrolyte containing 50 g dm^{-3} Zn, 200 g dm^{-3} H_2SO_4, and 0.08 mg dm^{-3} Sb^{3+}. (a) Sparged and (b) not sparged.

and larger in the non-sparged system. The observed decrease in grain size (facet size) in the sparged system would appear to be contrary to the behaviour reported by Winand [16]. However, the increased mass transfer in this case enhances the antimony effect which then dominates the observed morphology. The increase in K_{Zn} is a consequence of the antimony.

3.3. *Effect of acid concentrations*

Figure 10 shows the effect of sulphuric acid concentration on δ_{Zn} at current densities from 12 to 60 mA cm^{-2} for an antimony-free Zn electrolyte containing 50 g dm^{-3} Zn. The results indicate that the increase in acid concentration decreases δ_{Zn}, for example at 40 mA cm^{-2} the δ_{Zn} values are 3.63×10^{-3} and 3.27×10^{-3} cm for 100 and 200 g dm^{-3} H_2SO_4, respectively. Since the increase in H_2SO_4 concentration enhances the generation of hydrogen, there is a decrease in δ_{Zn}. The results obtained for antimony-containing electrolytes show a similar trend as for antimony-free electrolytes.

The K_{Zn} values, plotted versus Sb^{3+} concentration at a fixed current density of 60 mA cm^{-2} for sparged and non-sparged electrolytes, are shown in Figure 11 for 50 g dm^{-3} Zn electrolytes containing 100 and 200 g dm^{-3} H_2SO_4. The K_{Zn} values at both acid concentrations are increased significantly due to the sparging. For example, the K_{Zn} values are

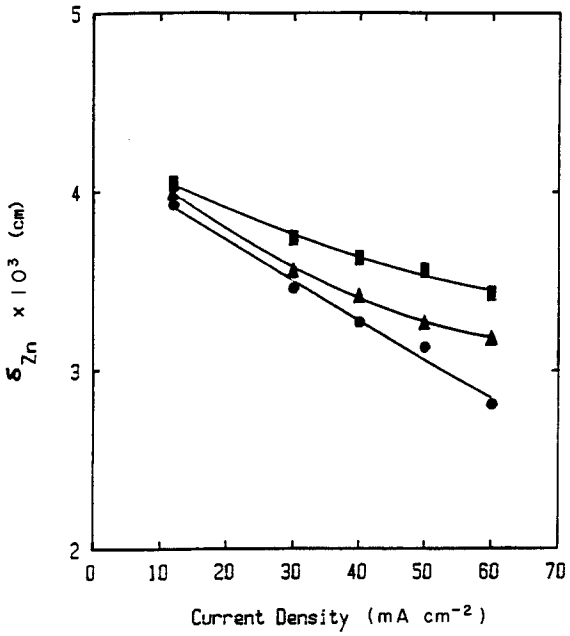

Fig. 10. The δ_{Zn} values obtained at different acid concentrations and current densities for a sparged electrolyte containing 50 g dm^{-3} Zn and antimony-free. (■) 100, (▲) 150 and (●) 200 g dm^{-3}, H_2SO_4.

14.84×10^{-4} for the sparged system and 6.99×10^{-4} cm s^{-1} for the non-sparged system for a 50 g dm^{-3} Zn electrolyte containing 200 g dm^{-3} H_2SO_4 and 0.06 mg dm^{-3} Sb^{3+}. The average increase in K_{Zn} from non-sparged to sparged systems is approximately a factor of 20 for 100 g dm^{-3} H_2SO_4 in the same antimony concentration range. Sparging also is effective at different current densities, as shown in Fig. 12, where the current density changes from 30 to 60 mA cm^{-2}. The results plotted in Fig. 12 are for an

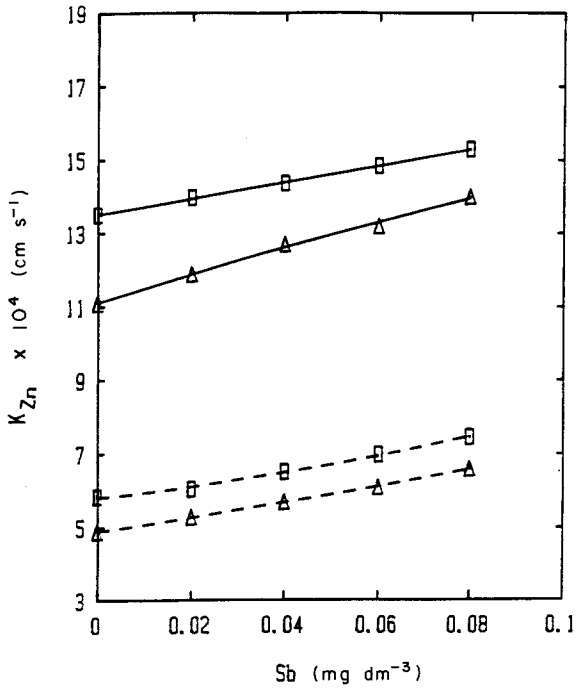

Fig. 11. The effect of acid concentration and Sb^{3+} concentration on sparged (——) and non-sparged (– – –) electrolytes containing 50 g dm^{-3} Zn at a 60 mA cm^{-2} current density. (△) 100 and (□) 200 g dm^{-3} H_2SO_4.

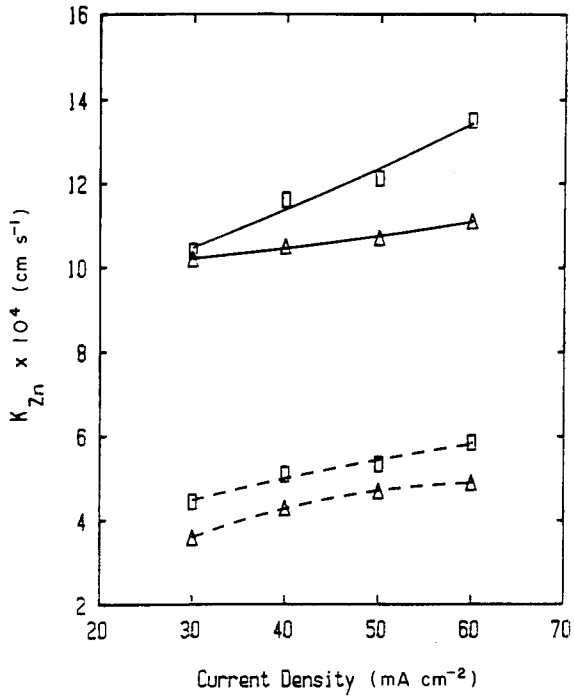

Fig. 12. The effect of sparging on the K_{Zn} values for an antimony-free electrolyte containing 50 g dm^{-3} Zn with (△) 100 and (□) 200 g dm^{-3} H_2SO_4. (——) Sparged and (– – –) non-sparged.

antimony-free electrolyte with 50 g dm^{-3} Zn, and at 100 and 200 g dm^{-3} H_2SO_4 concentration. The K_{Zn} is 11.61×10^{-4} cm s^{-1} for the sparged system at 40 mA cm^{-2} with 50 g dm^{-3} Zn electrolyte containing 200 g dm^{-3} H_2SO_4 and for the non-sparged system at the same conditions it is 5.1×10^{-4} cm s^{-1}, less than half the value for the sparged system. The results shown in Fig. 11 also indicate that K_{Zn} for the sparged system increases moderately with increasing acid concentration, for example for a 50 g dm^{-3} Zn electrolyte containing 0.06 mg dm^{-3} Sb^{3+}, K_{Zn} is 14.84×10^{-4} and 11.1×10^{-4} cm s^{-1} for 200 and 100 g dm^{-3} H_2SO_4, respectively.

3.4. *Relationship between the K_{Zn}s for sparged and non-sparged systems*

Figure 13 shows the relation between the mass transfer coefficients for the sparged system, K_{Zn}, and the non-sparged system, K'_{Zn}, for an antimony-free electrolyte. The results are expressed by the equation

$$K_{Zn} = A(K'_{Zn})^{0.54} \quad (5)$$

where A is an experimental constant and equal to 0.071. The above equation provides a satisfactory correlation for the present experimental work, where the average deviation is less than 2%. The correlation presented in Equation 5 can be used to predict the enhancement in K_{Zn} due to sparging at relatively higher gas sparging rates. Nitrogen gas sparged in this study has a velocity of about 3×10^4 cm s^{-1}. Further studies are needed to determine the relation between K_{Zn} values at lower sparging rates. Figure 14 represents a data fitting for the mass transfer coefficients for the

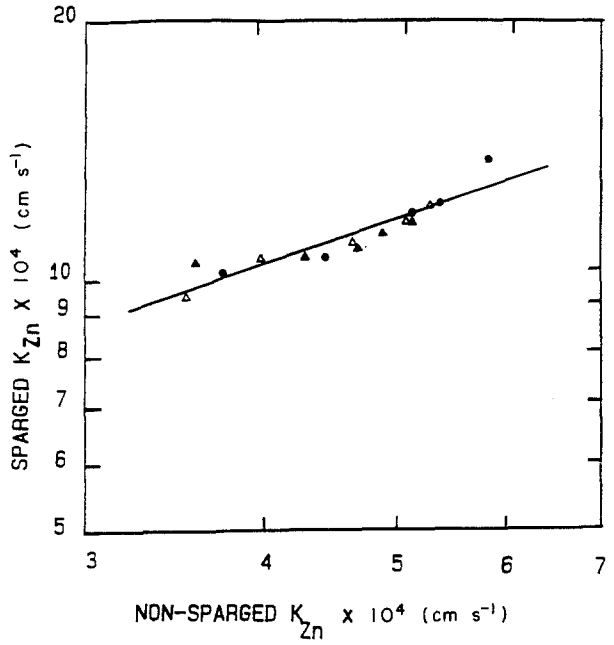

Fig. 13. An overall correlation between the sparged K_{Zn} and the non-sparged K_{Zn} for an antimony-free electrolyte with (○) 100, (▲) 150 and (△) 200 g dm^{-3} H_2SO_4.

sparged K_{Zn} and the non-sparged K'_{Zn} values for an electrolyte with antimony added at current densities varying from 12 to 60 mA cm^{-2}. The antimony concentration was varied from 0.02 to 0.08 mg dm^{-3} at acid concentrations of 100, 150, and 200 g dm^{-3}. The data fit the correlation described in Equation 5 very well; therefore, the relation between the sparged K_{Zn} and the non-sparged K'_{Zn} systems can be used effectively for further studies. The relation may apply to systems where a gas is evolving. In general, the correlation provides a simple and reliable relationship for calculating the enhancement in mass transfer due to sparging.

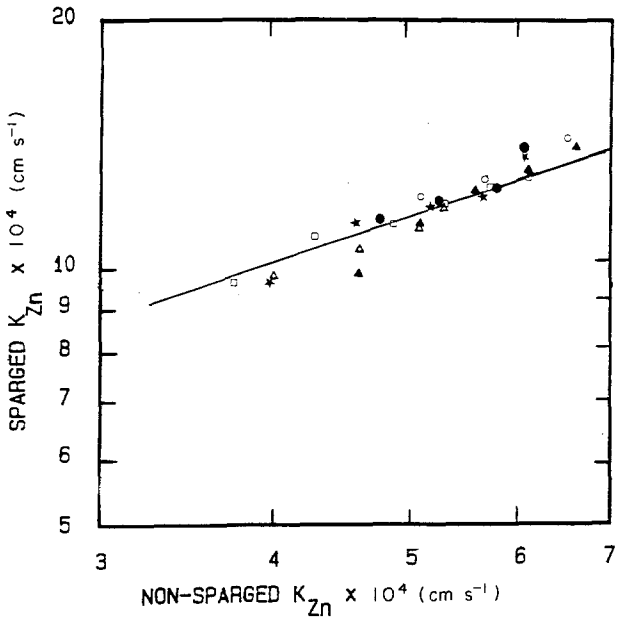

Fig. 14. Correlation fitting for the sparged K_{Zn} and the non-sparged K_{Zn} values for an electrolyte with antimony addition. [Acid]/g dm^{-3}, [Sb^{3+}]/mg dm^{-3}: (△) 100, 0.02; (▲) 100, 0.08; (□) 150, 0.02, (∗) 150, 0.04; (●) 200, 0.02; and (○) 200, 0.04, respectively.

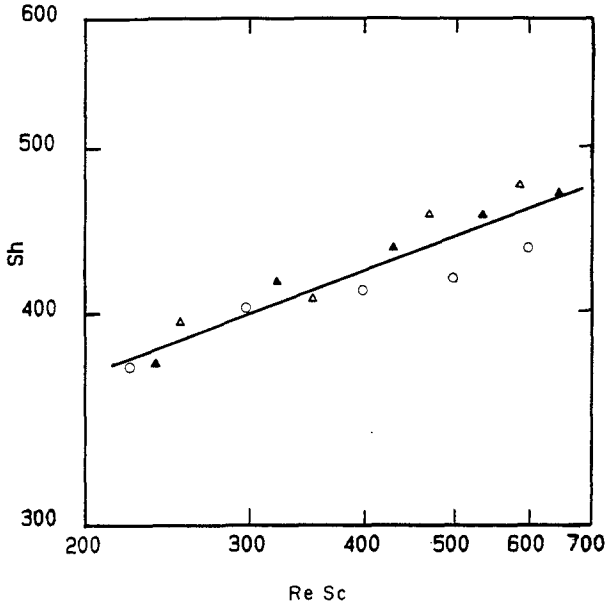

Fig. 15. Dimensionless representation of mass transfer results for an antimony-free electrolyte. (○) 100, (▲) 150 and (△) 200 g dm^{-3} H_2SO_4.

3.5. *Empirical correlation*

The mass transfer results for the sparged system are shown in Fig. 15 for an antimony-free electrolyte. The data can be expressed by the equation

$$Sh = a(ReSc)^{0.23} \quad (6)$$

where a is an experimental constant equal to 105. The equation above provides a satisfactory correlation for the present experimental data, where the average deviation is 2.1%. The correlation is envisaged in the dimensionless terms, *Re*, *Sh*, *Sc*, and, accordingly, the values of these groups are calculated. Physical properties used in the calculations were obtained from data available in the literature. For example, D_{Cd} was found to be 3.1 × 10^{-6} cm^2 s^{-1} [2], D_{Zn} = 3.8 × 10^{-6} cm^2 s^{-1} [17]. C_i is the concentration of Zn at the electrode/electrolyte interface and was calculated from the equation

$$I = nFK(C_b - C_i)/(1 - t) \quad (7)$$

The t values, transport number, were 0.055, 0.036, and 0.039 for a 50 g dm^{-3} Zn electrolyte containing 100, 150, and 200 g dm^{-3} H_2SO_4 respectively. ρ is the average density value in the electrolyte and equals $(\rho_b + \rho_i)/2$, where ρ_b represents the density in the bulk and ρ_i the density in the electrode/electrolyte interface. v is the average viscosity value in the electrolyte with concentration of C_b and C_i, equal to $(v_b + v_i)/2$. The v_b and v_i were determined from correlations based on the zinc ion concentration at the electrode surface. The *Sh* number was calculated using a 1.5 cm electrode length and experimental K_{Zn} and D_{Zn} values. The *Sc* number (v/D) was calculated using K_{Zn} and D_{Zn} values. The *Re* number (vL/v) was calculated using 1.5 cm as a characteristic electrode length and the current efficiency data. The exponent, m = 0.23, obtained from Equation 5 represents a

specific model where the gas is sparged onto gas-evolving electrodes.

Attempts were made to represent the mass transfer data using the theoretical model described in [4]; however, the results do not agree with the model. The difference can be explained by the fact that the isotropic eddies, whose presence is essential for the model, are not satisfied due to the perforated tube used as a sparger. The hydrodynamic model by Janssen [5, 13, 18] has an m value of 0.33 compared to the present value of 0.23. The difference may be due to the effect of simultaneous gas evolution with sparging. The correlation presented in Equation 6 does not require determination of a gas void fraction, ε, which is a necessary parameter in the Ibl model [3]. Gas void fraction calculations are important for models involving gas sparged electrodes.

The correlation presented in this study should be helpful in industrial applications where gas is evolving at the electrode surface. The results suggest that the sparged gas has two effects. The first is to create a turbulent flow which enhances mass transfer by disturbing the diffusion layer. The second is to quickly sweep the bubbles generated at the electrode surface, by preventing coalescence of the bubbles which enhances mass transfer by forced convection.

The correlation obtained represents a case where the gas-evolving electrodes are sparged with a gas such as nitrogen. The empirical correlation developed in this study should be helpful in further comparative studies. The enhancement in zinc mass transfer due to sparging is encouraging and suggests that sparging be applied to other systems where gas evolves at the electrode. Factors such as the electrode length, cell design, sparger type, and gas flow rates need further investigation for the development of a general model.

4. Conclusions

It is found that there are significant increases in the mass transfer coefficients of zinc when the system is sparged. Comparative results with a non-sparged system show an enhancement in K_{Zn} for the same kinetic parameters of temperature, antimony, zinc and acid concentrations, and current density. The K_{Zn} values for the sparged system is at least twice those for the non-sparged system. This suggests that sparging is an effective method for enhancing mass transfer. The diffusion layer thickness decreases significantly due to the turbulent conditions developed by the sparging. Increases in antimony concentration, acid concentration, and current density decrease the diffusion layer thickness of the sparged system, due to the fact that hydrogen is simultaneously evolved at the electrode surface. The δ_{Zn} values decrease from 18 to 25% when the antimony level is increased from 0.0 to 0.08 mg dm^{-3} or the current density is increased from 12 to 60 mA cm^{-2} at different acid concentrations. Similar results are noticed when the acid concentration is increased from 100 to 20 g dm^{-3} at a fixed antimony level and current density.

There is a definite change in the deposition morphology for the sparged system associated with the increase in current density from 20 to 80 mA cm^{-2}. The layer structure formed at low current densities changes to a more compact structure at higher current densities. There is also a change in the deposition morphology between the sparged and non-sparged systems especially in the presence of antimony. More rounded edges and a relatively compact structure are observed for the sparged systems.

A relationship between K_{Zn} for sparged and non-sparged systems is presented for a synthetic zinc electrolyte. The equation correlates the experimental data satisfactorily and provides a simple and reliable equation for a quick evaluation of the mass transfer coefficients in zinc electrowinning.

An empirical correlation envisaged in terms of the *Sh*, *Re*, and *Sc* numbers agrees very well with experimental mass transfer data for a synthetic zinc electrolyte. The correlation has an exponent, m, of 0.23. The correlation should be helpful for industrial applications. The correlation provides an important and novel approach for calculating the enhancement in mass transfer for gas-evolving electrodes sparged by an inert gas such as nitrogen.

References

[1] W. R. Johnson and L. E. Pfister, The Fourth AES Continuous Strip Plating Symposium, American Electroplater's Society, Inc., Winter Park, FL, May (1985) D1.
[2] S. F. Chen, PhD Dissertation, University of Missouri-Rolla (1986) pp. 55–84.
[3] L. Sigrist, O. Dossenbach, and N. Ibl, *Int. J. Heat Mass Transfer* **22** (1978) 1393–9.
[4] G. H. Sedahmed, *J. Appl. Electrochem.* **15** (1985) 777.
[5] H. Vogt, in 'Comprehensive Treatise of Electrochemistry', Vol. 6 (edited by E. Yeager, J. O'M Bockris, B. E. Conway, and S. Sarangapani), Plenum Press, New York (1983) p. 445.
[6] V. A. Ettel, B. V. Tilak, and A. S. Gendron, *J. Electrochem. Soc.* **121** (1974) 867.
[7] G. H. Sedahmed, H. A. Farag, A. A. Zatout, and F. A. Katout, *J. Appl. Electrochem.* **16** (1986) 374.
[8] G. H. Sedahmed and L. W. Schmilt, *Can. J. Chem. Eng.* **60** (1982) 767.
[9] G. H. Sedahmed, *J. Appl. Electrochem.* **8** (1978) 399.
[10] *Idem, ibid.* **10** (1980) 351.
[11] S. Mohanta and T. Z. Fahidy, *ibid.* **7** (1977) 235.
[12] J. R. Cuzmar, PhD Dissertation, University of Missouri-Rolla (1985) pp. 47–108.
[13] L. J. J. Janssen and J. G. Hoogland, *Electrochim. Acta* **18** (1973) 543.
[14] A. Y. Hosny, PhD Dissertation, University of Missouri-Rolla (1987).
[15] H. Vogt, *Electrochim. Acta* **23** (1978) 203.
[16] R. Winand, Electrocrystallization, in 'Application of Polarization Measurements in the Control of Metal Deposition' (edited by I. H. Warren) Elsevier Science, Amsterdam, The Netherlands (1984) pp. 47–83.
[17] E. W. Washburn, 'International Critical Tables', McGraw-Hill, New York (1929) 65.
[18] L. J. J. Janssen and J. G. Hoogland, *Electrochim. Acta* **15** (1970) 1013.